Impacts of Diurnal Cycle of SST on the Intraseasonal Variation of Surface Heat Flux over the Western Pacific Warm Pool①

Li Wei (李 薇), Yu Rucong (宇如聪),
Liu Hailong (刘海龙) and Yu Yongqiang (俞永强)
LASG, Institute of Atmospheric Physics, Chinese Academy of Sciences, Beijing 100029

(Received September 1, 2000)

ABSTRACT

Based on the method of estimating the diurnal amplitude of sea surface temperature (SST) as a function of daily averaged wind speed, precipitation and peak surface radiation, a parameterization scheme of diurnal cycle of SST is developed in the present study. Integrations to National Center for Atmospheric Research (NCAR) Community Climate Model (CCM3), separately forced by observed weekly SSTs with and without diurnal cycle of SST, are compared. Surface observation obtained from the Improved Meteorology (IMET) buoy during TOGA COARE Intensive Observation Period is applied to verify the SST parameterization, as well as a validation to the results from the CCM3 simulation. It is shown that the superposition of diurnal cycle of SST to the forced weekly SST makes a more realistic representation of the surface structure of intraseasonal oscillation over the western Pacific warm pool.

Key words: Diurnal cycle of SST, Surface heat flux, Intraseasonal oscillation

1. Introduction

One of the most important finding from TOGA (Tropical Ocean–Global Atmosphere) COARE (Coupled Ocean–Atmosphere Response Experiment) is the significant surface forcing (fluxes of momentum, heat and fresh water) related to the Madden–Julian Oscillation (MJO) and the corresponding response in upper ocean (Zhang, 1999a). The surface forcing components are highly coherent in structure and propagate eastward with the same speed of the MJO (Hendon and Glick, 1997; Jones and Weare, 1996). The MJO strongly affects the heat balance within the upper layer of equatorial Indian Ocean and the western Pacific, which is manifested on the intraseasonal variation of sea surface temperature (SST). It has been found in the observation that the intraseasonal SST anomaly moves across the Indian Ocean out past the date line with a phase lag of 1 / 4 period to the center of intraseasonal anomaly of deep convection (Zhang, 1996; Hendon and Glick, 1997). Either latent heat or solar radiation heat fluxes at the surface contributes to the intraseasonal variation of SST (Hendon and Glick 1997; Shinoda et al., 1998). Sun et al. (1993) also demonstrated that there are significant oscillations of surface heat flux and SST on the intraseasonal time scale over warm pool and there may be close connection between them.

①This study was sponsored by Chinese Academy of Sciences under Grant "Hundred Talents" for "Validation of Coupled Climate Models" and the National Natural Science Foundation of China under Grant No. 40023001.

While evidences of intraseasonal atmospheric forcing and oceanic response are convincing, whether and how such oscillation of SST may feed back the atmosphere on the same time scale are not yet clear. It was estimated by Shinoda et al. (1998) using a global model analysis data set that the intraseasonal SST variation significantly reduces the amplitude of the latent and sensible heat fluxes. With regard to the influence of intraseasonal SST fluctuation on the MJO structure, there are only some evidences from numerical studies. The simulated MJO has a more reasonable intensity, period and propagating speed if SST fluctuates responding to the variation of surface heat flux (Flatau et al., 1997; Waliser et al., 1999).

It is understandable that the ocean does not necessarily feed back to the atmosphere on the same timescales as it is disturbed. Cross–scale air–sea interaction may exist (Sui et al. 1997). Over the western Pacific warm pool where the MJO is most active, SST was observed to fluctuate at two disparate timescales: intraseasonal and diurnal (Weller and Anderson, 1996). The most possible scenario of cross–scale SST feedback to the MJO is accordingly through the diurnal cycle (Zhang, 1999b), although it has not been well documented. In the present study, results from two integrations of National Center for Atmospheric Research (NCAR) Community Climate Model (CCM3) (Kiehl et al., 1998), separately forced by the observed weekly SSTs with and without the parameterized diurnal cycle, are compared to investigate the feedback of diurnal cycle of SST to the intraseasonal variation of surface heat flux, which is the pilot study to the understanding of interaction between the diurnal cycle of SST and the MJO. Buoy observations from TOGA are applied as the verification data.

The significance and parameterization scheme of the diurnal cycle of SST are described in Sections 2 and 3, respectively. Section 4 provides information on the CCM3 experiments and verification data. The results are presented and discussed in Section 5. Section 6 summarizes the results.

2. The significance of diurnal cycle of SST

Diurnal cycle is one of the most important periods of SST variation over the warm pool. The mean amplitude of diurnal variation of SST is 1°–2°C and may reach as high as 3.8°C under calm clear conditions over the tropical western Pacific (Fairall et al., 1996a), which is much remarkable in comparison with the amplitude of intraseasonal variation of local SST (0.25°C) (Shinoda et al., 1998). Using the hourly data averaged for 5 buoys around (0°, 156°E) for the period 1 September 1992 to 28 February 1993, the percentages of variance explained by oscillation of SST with different period are calculated and listed in Table 1.

Table 1. The percentage of variance of SST oscillation with different period around 0°, 156°E based on buoy data from TOGA COARE

Period (T) (unit: day)	$T>60$	$60>T\geqslant 30$	$30>T\geqslant 14$	$14>T\geqslant 7$	$7>T\geqslant 2$	$2>T\geqslant 1/12$
Percentage of variance	31.8%	21.3%	7.6%	10.5%	5.8%	23.0%

Because of the high mean temperature in tropical ocean and Clausius–Clapeyron relationship, the diurnal cycle of SST has significant impact on the surface fluxes of latent and sensible heat (Hall and Haar, 1999). A 1°C change in SST results in a variation of 27 W m^{-2} to the net surface heat flux over the warm pool (Webster et al., 1996). The diurnal cycle forms a significant period to the interaction between tropical ocean and atmosphere (Zhang, 1996).

The diurnal variation of SST is closely related to the complicated processes such as diurnal cycle of solar radiation, cloud–radiation coupling and cloud–SST coupling. The accurate observation and reproducing of the diurnal cycle of SST is indispensable to the correct understanding and description of the air–sea coupling system over the warm pool. The lack of a fundamental process of SST feedback to the atmosphere on short timescales may partly account for the error in the simulation of large–scale cloud and atmospheric activity (Webster et al., 1996). The diurnal cycle of SST derived from the surface heat flux is superposed to the SST forcing in integration of CCM3 in the present study.

3. Parameterization of diurnal cycle of SST

The ultimate forcing of the diurnal variation of SST comes from the diurnal cycle of solar radiation. The surface wind speed is also of importance to the diurnal variation of SST by altering the latent heat flux. Additionally, fresh water from precipitation makes a stable layer in the upper ocean, which favors the increase of SST. A method to determine the amplitude of diurnal cycle of SST based on the maximum of solar radiation within one day, daily mean surface wind and precipitation was proposed by Webster et al. (1996). The empirical constants quantified by Webster et al. (1996) are employed in the present parameterization scheme of diurnal cycle of SST. The essentials of the parameterization are described as follows. The daily mean value of SST is kept changeless when the parameterized diurnal variation is introduced. The variation of SST is determined by the solar radiation and surface wind one hour before it. The SST maximum appears one hour after the peak of solar radiation during the daytime while the SST minimum appears at the local dawn.

Let us set that D denotes the time series. D_h^j represents the hth hour on jth day. $h \in [1,2,\cdots,23,24]$ and $h=1$ is defined as the time at the local sunset.

The diurnal variation of SST is

$$\Delta T_{D_h^j} = \Gamma_{D_h^j}(S_I,U) - \frac{1}{12}\sum_{h=1}^{24}\Gamma_{D_h^{j-1}}(S_I,U)\cdot\left(1-\frac{|12-(h-1)|}{12}\right)$$

$$\Gamma(S_I,U) = \begin{cases} a+b*S_I+c*\ln(U)+d*S_I*\ln(U)+e*U & S_I>0 \\ 0 & S_I\leqslant 0 \end{cases}$$

where $\Delta T_{D_h^j}$ is the variation of SST at the time of D_h^j. S_I is the downwelling solar radiation (unit: W m^{-2}). U is the surface wind speed (unit: m s^{-1}). Following Webster et al. (1996), the constants of a, b, c, d, e are 0.262, 0.00265, −0.838, −0.00105, 0.158, respectively, on the condition $U>2$ and 0.328, 0.002, 0.212, −0.000185, −0.329, respectively, on the condition $U\leqslant 2$. $\sum_{h=1}^{24}\Gamma_{D_h^{j-1}}$ is the sum of Γ in day $j-1$.

Hourly surface variabilities measured by Improved Meteorology (IMET) buoy (1.75°S,156°E) (Anderson et al., 1996) during TOGA COARE Intensive Observation Period (IOP, 1 November 1992–28 February 1993) are utilized to verify the parameterization of diurnal cycle of SST and the comparison is shown in Fig. 1. In Fig. 1a, the daily means of observed SST without (solid curve) and with (dashed curve) the parameterized diurnal variation are consistent during the IOP. The consistency confirms that the daily mean value is kept. The diurnal anomaly of the observed SST (solid) and calculated one (dashed) are given in Figs. 1b and 1c, respectively. It can be seen that the parameterization correctly reproduces the features of diurnal variation of SST with respect to both amplitude and phase.

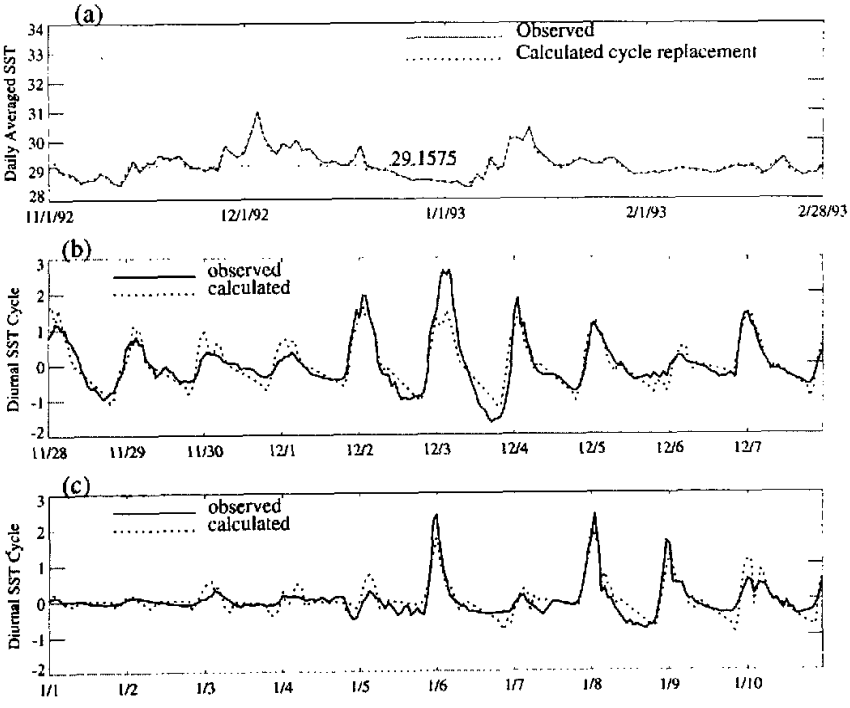

Fig. 1. Validation of the parameterized diurnal cycle of SST (dashed) on the basis of IMET buoy observation (solid) during TOGA COARE IOP (1 November 1992–28 February 1993). a. Comparison of the daily mean through the entire period; b. Comparison of diurnal anomaly during 28 November–8 December 1992; c. Comparison of diurnal anomaly during 1 January–11 January 1993.

4. Experiments and verification data

Two experiments of NCAR CCM3, with the same initial condition, are carried out to examine the influence of diurnal cycle of SST upon the simulated MJO in the tropics. CCMW integration is forced by daily mean SST, which is obtained by linearly interpolating the weekly SST (Reynolds and Smith 1994). In CCMD integration, a diurnal cycle parameterized by the predicted surface wind and shortwave radiation is superposed to the daily SST. In other words, there is a feedback of SST to the surface fluxes of heat and momentum on timescale shorter than one day. Strictly speaking, SST is not a real forcing field in CCMD.

Daily data from CCMW and CCMD for period 1982 to 1992 are compared. The intraseasonal variability is identified by filtering the data with bandpass (30–90 days) filter. Empirical Orthogonal Function (EOF) analysis and harmonic analysis are also employed in the present studies. A 7–day mean to the daily data has been calculated before the bandpass filter. It has been verified that there is little difference to the bandpass filtered results between the daily and 7–day mean data.

The surface variabilities measured by IMET buoy involve wind vector, air temperature, SST, relative humidity, precipitation, shortwave radiation and longwave radiation. The avail-

able time series are from 22 October 1992 to 3 March 1993. Fluxes of sensible heat (Q_s) and latent heat (Q_l) are calculated applying the TOGA COARE bulk formula (version 2.5b)(Fairall et al., 1996b). The net downwelling heat flux (Q_{down}) is the total energy that ocean gets from the surface, which consists of four components

$$Q_{down} = Q_{sw} - Q_s - Q_l - Q_{lw},$$

where $Q_{sw} = (1-\alpha)Q_{sw0}$ is the downwelling solar radiation flux into the ocean, Q_{sw0} is the observed incoming solar radiation and $\alpha = 0.06$ is the surface albedo. Q_{lw} is the observed longwave radiation.

The upwelling heat flux (Q_{up}) is the total energy that atmosphere gets from the surface, taking the form as

$$Q_{up} = Q_s + Q_l + Q_{lw} + \alpha Q_{sw0}.$$

The pentad CMAP precipitation is obtained by merging gauge, 5 kinds of satellite estimates and numerical model predictions (Xie and Arkin, 1997), with the grid resolution of 2.5° × 2.5°. The CMAP data are averaged over 1982–1992 to validate the simulated climatology in both CCMW and CCMD.

5. Results

5.1 *Reproducing of the climatology*

Figures 2a and 2b show the 11-year means (1982–1992) of precipitation from CMAP data and from CCMW simulation, respectively. One can see that CCMW captures the salient features of the climatic structure in the observation. The precipitation centers locating at the warm pool and equatorial Indian Ocean are correctly represented, with a reasonable peak of about 9 mm / day. The climatology in CCMD (not shown) has a good agreement with that in CCMW, which can be deduced from the small difference of mean precipitation between CCMD and CCMW (Fig. 2c). Positive value in Fig. 2c denotes that the precipitation from CCMD is greater than that from CCMW. It is detected that the main differences lie in the tropical ocean where the annual mean precipitation is relatively larger, especially over the Indian Ocean and the western Pacific. The maximum of the difference is not greater than 1 mm / day, which means 10% of the mean value from CCMW. According to Fig. 2, it is verified that both CCMW and CCMD do a reasonable job in representing the average climate. The changes in the characteristics of the simulated intraseasonal variability between two integrations is not due to the discrepancy in the background climate.

5.2 *EOF analysis of the intraseasonal precipitation over the tropical western Pacific*

It is evident in Fig. 2c that the tropical western Pacific must be a focus of attention for the comparison between CCMW and CCMD. The influence of diurnal variation of SST on the intraseasonal precipitation is further examined in this region.

Figures 3a and 3b show the dominant modes of intraseasonal variability (30–90 day filtered) in the simulated precipitation from CCMW and CCMD over the tropical western Pacific (10°S–10°N, 135°E–180°) for 1982–1992, as described by EOF analysis. EOF1 explains 14.5% / 18.5% of the variance in CCMW / CCMD. The structures of EOF1 modes in CCMW and CCMD are analogous with two centers of intraseasonal precipitation north and south of the equator.

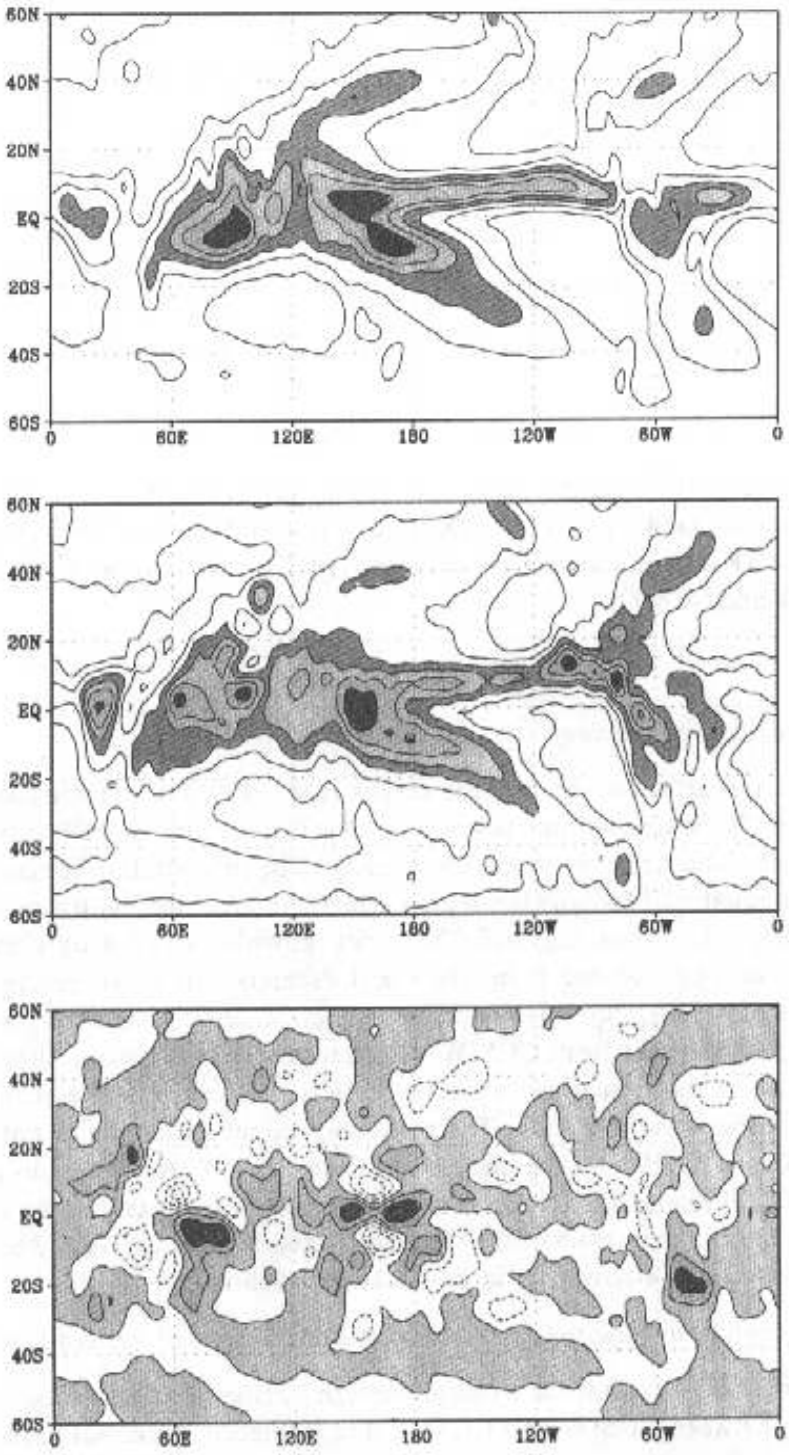

Fig. 2. The 11-year means (1982–1992) of precipitation from CMAP data (a), and from CCMW simulation (b), respectively. Contour interval is 1.5 mm / day. Value over 4.5 mm / day is shaded. Also given is the difference of mean precipitation between CCMD and CCMW (c). Contour interval is 0.2 mm / day. The shaded positive value means CCMD is greater than CCMW.

The time series of the principal components (PCs) of the EOF1 of intraseasonal precipitation from CCMW and CCMD are shown in Fig. 3c. The tendency of the long term variability of two intraseasonal PCs is coherent (e.g., the weakest intraseasonal anomaly occurs in

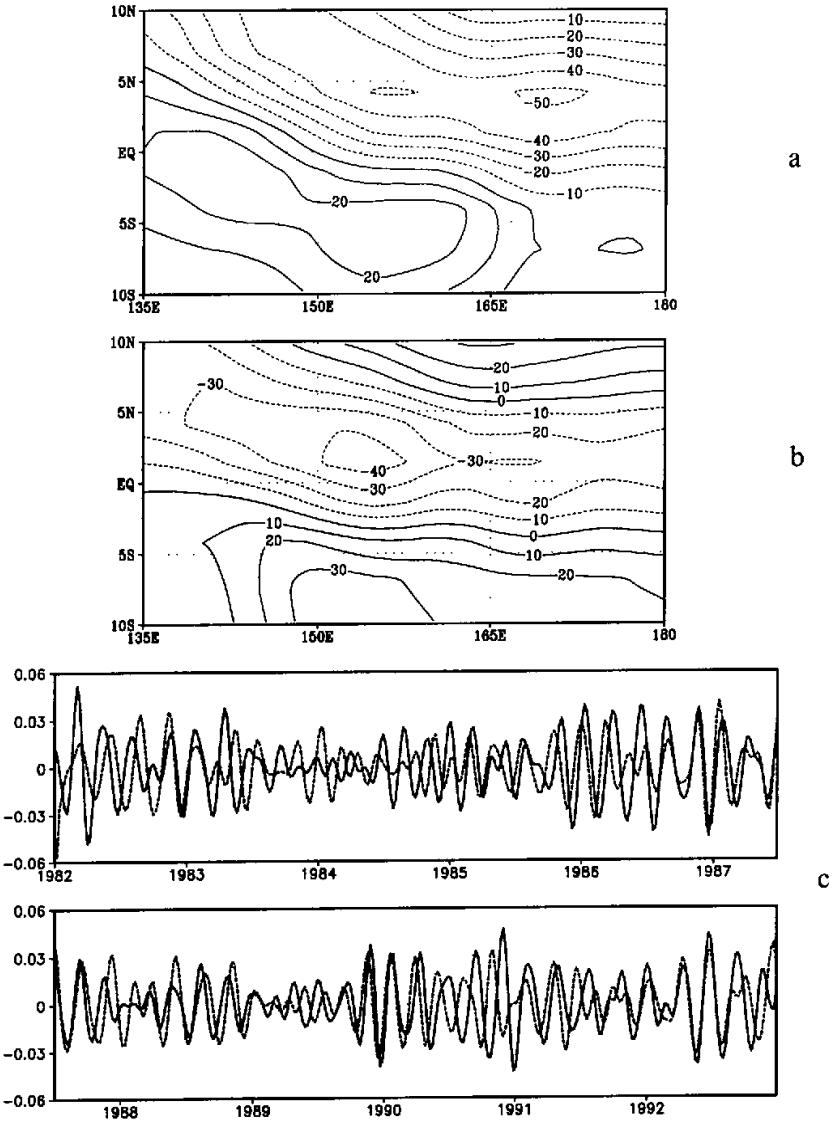

Fig. 3. Dominant modes of intraseasonal variability (30–90 day filtered) in the simulated precipitation from CCMW (a) and CCMD (b) in tropical western Pacific (10°S–10°N, 135°E–180°) for 1982–1992, as described by EOF analysis. The time series of PC1s from CCMW (dashed) and CCMD (solid) are shown in (c).

1989 in both PCs) while there are distinct phase differences in some periods such as summer–fall in 1982 and summer–fall in 1990.

The correlation of two PCs is calculated to examine their phase relationship. The most significant correlation (0.34) is at 7 days lag. With the length of time series of 574 (7–day averaged beforehand), correlation coefficient 0.34 is beyond the significance level at 95% confi-

dence. It can be deduced that with all the similarities in the structure of EOF1s and long term variability of PCs, there is obvious phase difference between the dominant modes of intraseasonal precipitation from CCMW and CCMD. The phase difference is important to the MJO simulation as it reflects the different surface structures, which imply the different processes of the MJO to get energy from the surface.

5.3 *Surface structure of the MJO in the observation*

The knowledge to the surface structure of the MJO is inconsistent among the existing researches. Two types of surface structures have been observed (Zhang and McPhaden, 1999). The first model is based on wave–CISK (convective instability of the second kind) theory (e.g., Lau and Peng, 1987) and places a center of atmospheric deep convection and associated maximum precipitation in between the surface maximum easterlies to the east and maximum westerlies to the west. The amplitude of the westerlies is greater than that of the easterlies. Both observation (Flatau et al., 1997) and model analyses (Jones and Weare, 1996) offer evidences of this type of configuration. The second model differs from the first mainly on that the location of maximum westerlies is within the convective center rather than to its west. This model has also been reported in both observation (Zhang, 1996; Cronin and McPhaden, 1997) and model analyses (Shinoda et al., 1998). It was pointed out by Zhang and McPhaden (1999) that the surface structure of the MJO may be suggestive of different air–sea interaction processes.

The phases of surface fluxes of heat and momentum, convection and SST within the period of MJO are investigated in an observed case study. Daily mean surface variabilities are obtained from hourly data of IMET buoy from 22 October 1992 through 3 March 1993. The time series of observed SST, precipitation, Q_{sw}, Q_{lw}, Q_{lh}, Q_{sh}, Q_{down}, Q_{up} and surface wind speed are shown in Fig. 4 (only harmonics with periods 33–66 days are involved). The signals of intraseasonal variation are obvious in each surface variabilities corresponding to the three well known MJO events during the IOP, which center in early November 1992, late December 1992 and late January to early February 1993, respectively (Godfrey et al., 1998). A composite is constructed to explore the common characteristics of the phase relationship of surface variabilities. The center of the MJO is defined as the day of minimum SST (negative anomaly) in the three MJO events, i.e., 15 November 1992, 28 December 1992 and 7 February 1993. A 20 days interval prior to and posterior to each center day is taken to make the composite of 41 days in length.

The MJO composite based on IMET data is shown in Fig. 5. With 0 day fixed on the minimum, the amplitude of intraseasonal variation of SST is 0.4°C during the course of 41 days. There is rise and fall of SST before and after 0 day, respectively. The peak of intraseasonal precipitation occurs at −7∼ −8 day. The minimum of intraseasonal precipitation is seen at +13 day. Among all components of the heat flux, the intraseasonal variabilities in longwave radiation and sensible heat flux are weak and not worth particular discussion. Around −4∼ −5 day, shortwave radiation reaches its minimum whilst latent heat gains its maximum. Both of them have the amplitude close to 20 W m^{-2}. The anomaly of net downwelling heat flux is hence largest (about −34 W m^{-2}) at that time. The intraseasonal variabilities of latent heat flux and surface wind speed are nearly in phase, reflecting the former is modulated by the later to great extent. The peak upwelling heat flux is found at −5 day and is controlled mainly by the latent heat flux (wind speed). The process of the composite MJO is summarized in Table 2.

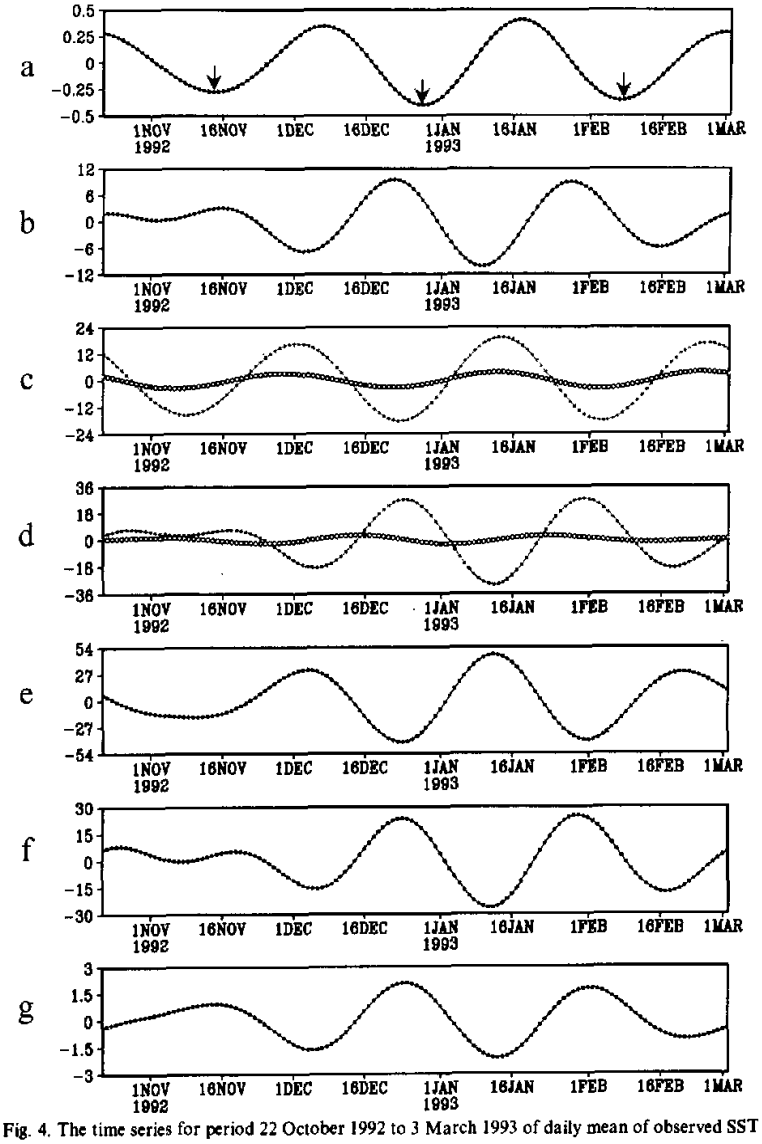

Fig. 4. The time series for period 22 October 1992 to 3 March 1993 of daily mean of observed SST (a), unit:°C), precipitation (b), unit: mm / day), Q_{sw} and Q_{lw} (c), Q_{lh} and Q_{sh} (d), Q_{down} (e), Q_{up} (f) and surface wind speed (g), unit: m s^{-1}). Only harmonics with periods 33–66 days are involved. Unit for heat flux is W m^{-2}. Q_{lw} and Q_{sh} are denoted by open circles in (c) and (d), respectively. The arrows in (a) denote the three centers of negative anomaly of intraseasonal SST.

The phase relationship revealed in the composite from IMET data is consistent with the results from observational studies by Flatau et al. (1997), i.e., the peak of intraseasonal precipitation precedes the maximum wind speed and latent heat flux by about 3 days. Considering the fact that the convectional anomaly propagates eastward over the warm pool (Godfrey

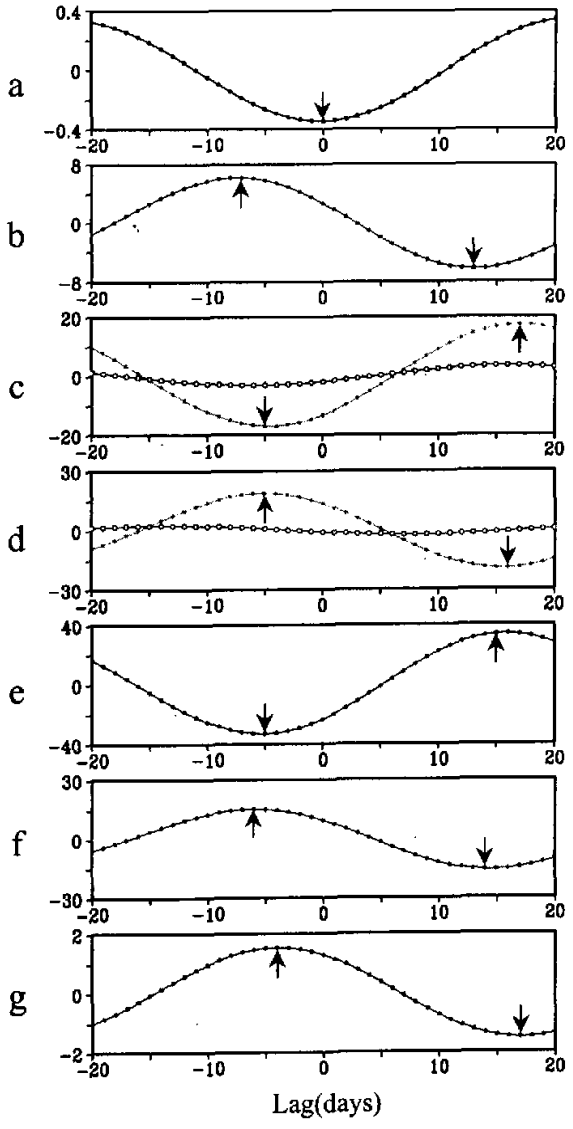

Fig. 5. Profiles taken from composite of IMET buoy. The order of panels is same as in Fig.4. Arrows denote the time of peak.

et al., 1998), this configuration is identical to the first type of surface structure aforementioned. The heaviest precipitation is about 7 days ahead the negative anomaly of SST and about 13 days behind the positive anomaly of SST.

5.4 Surface structure of the MJO in CCM simulations

The intraseasonal variation of the weekly SST to force CCM3 (averaged of grid points of 1.40°S, 154.69°E and 1.40°S, 157.50°E) has consistent phase with that from IMET buoy. Taking the same center days as those of the IMET composite, the composites constructed from CCMW and CCMD data are shown in Figs. 6 and 7, respectively. It can be seen that there are obvious differences in the phases of the convection activities and surface variabilities in the two composites. Validated by the IMET data, the simulated phase relationship is found to be more realistic in CCMD than in CCMW. The phases of the peaks of longwave radiation, latent heat, net downwelling heat flux, surface wind and upwelling heat flux show very good agreement between CCMD simulation and IMET data. In contrast, the error in the simulated latent heat flux, which is mainly dependent on the surface wind, is the major reason for the unrealistic phase in the heat flux in CCMW. The wind speed reaches its maximum at −15 day.

Table 2. Process of composite MJO from IMET buoy data. The (P) and (N) mean the centers of positive and negative anomalies, respectively

Day −8~−7		Day −5~−4		Day 0		Day +13		Day +15~+17
Precipitation (P)	→	Shortwave radiation (N)	→	SST (N)	→	Precipitation (N)	→	Shortwave radiation (P)
	→	Latent heat flux (P)					→	Latent heat (N)
	→	Net downwelling heat flux (N)					→	Net downwelling heat flux (P)
	→	Upwelling heat flux (P)					→	Upwelling heat flux (N)
	→	Surface wind speed (P)					→	Surface wind speed (N)

The phase of shortwave radiation is not as accurate as other variabilities in CCMD, although it is more reasonable than that in CCMW. It is noted that the magnitude of this term (about 4 W m^{-2}) is much smaller than that in the observation (about 18 W m^{-2}), making relative smaller contribution to the net heat flux. The intensity of the intraseasonal variability of precipitation is smaller in both simulations. Consistent with the observation, the maximum of precipitation leads while the minimum of precipitation lags the center of negative anomaly of SST (0 day). But it is not the case of CCMW. It confirms the results from EOF analysis (Fig. 3c) that there is strongest correlation of intraseasonal precipitation between CCMW and CCMD at lag of several days.

Comparison of each component of heat flux between CCMW and CCMD simulations show that, particularly to the latent heat, the magnitude simulated by CCMD are overall lower than that from CCMW. It was suggested by Shinoda et al. (1998) that the feedback of intraseasonal SST variation to surface heat flux is to reduce the amplitude of intraseasonal variation of latent / sensible heat flux. According to the CCM3 experiments, the feedback of diurnal variation of SST is also proved to reduce the intraseasonal latent heat flux at the surface during TOGA IOP. It is, however, the result from a case study in a limited period and some further examination is needed.

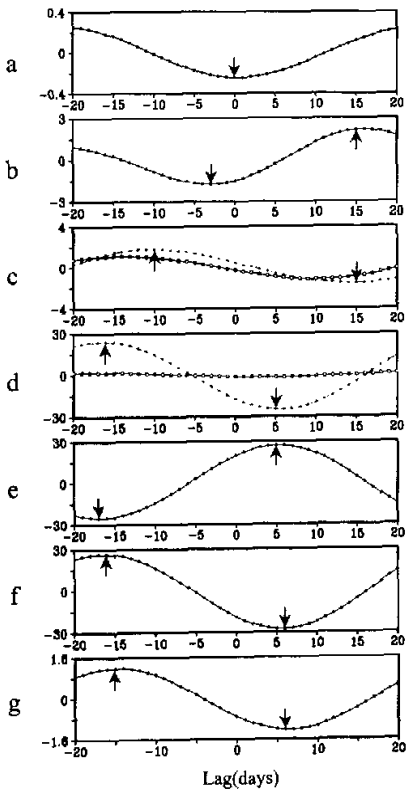

Fig. 6. Same as Fig.5, but for CCMW simulation.

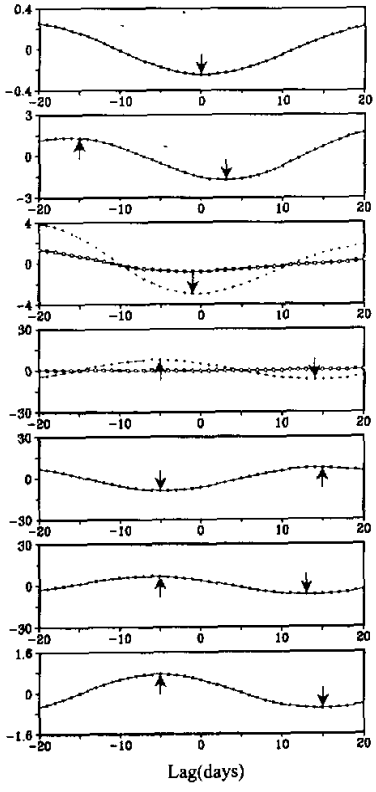

Fig. 7. Same as Fig.5, but for CCMD simulation.

6. Concluding remarks

Based on the method (Webster et al. 1996) of estimating the diurnal amplitude of SST, a parameterization scheme of diurnal cycle of SST based on the surface wind and shortwave radiations is developed in the present study. Surface observation obtained from the IMET buoy during TOGA COARE IOP is applied to verify the parameterization.

The parameterization of diurnal cycle of SST is applied to the forcing field of CCM3. CCMW and CCMD are separately forced by observed weekly SSTs without and with the diurnal cycle. EOF analyses to the simulated intraseasonal precipitation over the tropical western Pacific show that the correlation of PC1s from CCMW and CCMD is the strongest at 7 days lag.

Composite analysis shows that the feedback of diurnal cycle of SST is important to make a more realistic representation of the surface structure of intraseasonal oscillation over the western Pacific warm pool. As revealed in IMET data, there is positive anomaly of SST to the east and negative anomaly of SST to the west of the peak of intraseasonal precipitation. The phase relationship is more realistic represented in CCMD than that in CCMW. Among all the surface variabilities calculated by CCMD, the phases of intraseasonal variability of longwave

radiation, latent heat flux, net downwelling heat flux, surface wind and upwelling heat flux have excellent agreement with the observation. The feedback of diurnal variation of SST in CCMD reduces the intraseasonal latent heat flux at the surface during TOGA IOP.

REFERENCES

Anderson, S.P., R.A. Weller, and R.B. Lukas, 1996: Surface buoyancy forcing and the mixed layer of the western Pacific warm pool: Observations and 1-D model results. *J. Climate*, **9**, 3056–3085.

Cronin M. F., and M. J. McPhaden, 1997: The upper ocean heat balance in the western equatorial Pacific warm pool during September–December 1992. *J. Geophys. Res.*, **102**, 8533–8554.

Fairall, C. W., E. F. Bradley, J. S. Godfrey, G. A .Wick, J. B. Edson, and G.S .Young, 1996a: Cool-skin and warm-layer effects on sea surface temperature. *J. Geophys. Res.*, **101**, 1295–1308.

Fairall, C. W., E. F. Bradley, D. P. Rogers, J. B. Edson, and G. S. Young, 1996b: Bulk parameterization of air–sea fluxes for Tropical Ocean–Global Atmosphere Coupled–Ocean Atmosphere Response Experiment Algorithm. *J. Geophys. Res.*, **101**, 3747–3764.

Flatau, M., P. J. Flatau, P. Phoebus, and P. P. Niller, 1997: The feedback between equatorial convection and local radiative and evaporative processes: The implications for intraseasonal oscillations. *J. Atmos. Sci.*, **54**, 2372–2386.

Godfrey J. S. et al., 1998: Coupled Ocean–Atmosphere Response Experiment (COARE): An interim report. *J. Geophys. Res.*, **103**, 14,395–14,450.

Hall, T. J., and T. V. Haar, 1999: The diurnal cycle of west Pacific deep convection and its relationship to the spatial and temporal variation of tropical MCSs. *J. Atmos. Sci.*, **56**, 3401–3415.

Hendon, H. H., and J. Glick, 1997: Intraseasonal air–sea interaction in the tropical Indian Ocean and Pacific Oceans. *J. Climate*, **10**, 647–661.

Jones, C., and B. C. Weare, 1996: The role of low-level moisture convergence and ocean latent heat fluxes in the Madden and Julian oscillation: An observational analysis using ISCCP data and ECMWF analysis. *J. Climate*, **9**, 3086–3140.

Kiehl, J. T., J. J. Hack, G. B. Bonan, B. A. Boville, D. L. Williamson, and P. J. Rasch, 1998: The National Center for Atmospheric Research Community Climate Model: CCM3. *J. Climate*, **11**, 1131–1149.

Lau, K. M., and L. Peng, 1987: Origin of low-frequency (intraseasonal) oscillations in the tropical atmosphere. Part I. Basic theory. *J. Atmos. Sci.*, **44**, 950–972.

Reynolds, R. W., and T. M. Smith, 1994: Improved global sea surface temperature analyses using optimum interpolation. *J. Climate*, **7**, 929–948.

Shinoda, T., H. H. Hendon, J. Glick, 1998: Intraseasonal variability of surface fluxes and sea surface temperature in the tropical western Pacific and Indian Oceans. *J. Climate*, **11**, 1685–1702.

Sui, C. H., X. Li, K. M. Lau, and D. Adamec, 1997: Multiscale air–sea interaction during TOGA COARE. *Mon. Wea. Rev.*, **125**, 448–462.

Sun, Jilin, Wu Dexing and Xu Tianzhen, 1993: Analysis of intraseasonal variations of SST and air–sea fluxes during TOGA–COARE IOP. *J. Ocean University of Qingdao*, **23**(Special issue), 63–78 (in Chinese).

Waliser, D. E., K. M. Lau, and J. H. Kim, 1999: The influence of coupled sea surface temperatures on the Madden–Julian oscillation: A model perturbation experiment. *J. Atmos. Sci.*, **56**, 333–358.

Webster, P. J., C. A. Clayson, and J. A. Curry, 1996: Clouds, radiation, and the diurnal cycle of sea surface temperature in the tropical western Pacific. *J. Climate*, **9**, 1712–1730.

Weller, R. A., and S. P. Anderson, 1996: Temporal variability and mean values of the surface meteorology and air–sea fluxes in the western equatorial Pacific warm pool during the TOGA COARE. *J. Climate*, **9**, 1950–1990.

Xie Pingping, and P. A. Arkin, 1997: Global precipitation: A 17-year monthly analysis based on gauge observations, satellite estimates and numerical model outputs. *Bull. Amer. Meteor. Soc.*, **78**, 2539–2558.

Zhang Chidong, 1996: Atmospheric intraseasonal variability at the surface in the tropical western Pacific Ocean. *J. Atmos. Sci.*, **53**, 739–758.

Zhang Chidong, 1999a: Intraseasonal atmospheric surface forcing, ocean responses, and SST feedback in the equatorial western Pacific. In: *Proceedings of A Conference on the TOGA COARE*, WCRP-107 (WMO / TD-No. 940), 175-176.

Zhang Chidong, 1999b: Sensitivity of surface latent and sensible heat fluxes to intraseasonal fluctuations in tropical sea surface temperatures. *J. Atmos. Sci.* (submitted).

Zhang Chidong, and M. J. McPhaden, 2000: Intraseasonal surface cooling in the equatorial western Pacific. *J. Climate*, 13, 2261-2276.

SST 日变化对西太平洋暖池海表热通量季节内变化的影响

李 薇 宇如聪 刘海龙 俞永强

摘 要

基于利用日最大太阳辐射、日平均海面风和日降水量近似计算海表温度(SST)日变化的振幅的方法，发展了一个计算 SST 日循环的参数化方案. 利用周平均 SST 强迫美国国家大气研究中心(NCAR)的 CCM3 大气模式进行了有、无考虑 SST 日变化的比较试验. 热带海洋与全球大气计划之耦合海气响应实验(TOGA COARE)的强化观测期间 IMET 浮标的逐时海表观测资料不仅验证了该参数化方案的合理性，也表明了利用参数化方案对强迫场 SST 迭加日变化使 CCM3 较真实地模拟出西太平洋暖池海表热通量的季节内变化的位相结构.

关键词: SST 日变化，海表热通量，季节内振荡